



OPEN

Captopril supported on magnetic graphene nitride, a sustainable and green catalyst for one-pot multicomponent synthesis of 2-amino-4*H*-chromene and 1,2,3,6-tetrahydropyrimidine

Fatemeh Rezaei, Heshmatollah Alinezhad[✉] & Behrooz Maleki[✉]

Captopril (CAP) is a safe, cost-effective, and environmentally organic compound that can be used as an effective organo-catalyst. Functional groups of captopril make it capable to attach to solid support and acting as promoters in organic transformations. In this work, captopril was attached to the surface of magnetic graphene nitride by employing a linker agent. The synthesized composite efficiently catalyzed two multicomponent reactions including the synthesis of 1,2,3,6-tetrahydropyrimidine and 2-amino-4*H*-chromene derivatives. A large library of functional targeted products was synthesized in mild reaction conditions. More importantly, this catalyst was stable and magnetically recycled and reused for at least five runs without losing catalytic activity.

In recent years, employing advanced sustainable catalytic system have attracted much attention as a green approach to overcome environmental pollution¹. In this regard, bio-based catalytic systems have been introduced as promising compounds due to their nontoxicity, economy, biodegradability, and availability². Through numerous research reports, the participation of small drugs and biomaterials, with multiple functional groups, in catalytic systems to perform organic reactions such as C–C and C-heteroatom bond forming reactions, cyclization, Knoevenagel condensation, and Michael addition have attracted much attention^{3–6}.

One of the effective strategies to take advantage of these compounds and simultaneously benefit from the privilege of the heterogeneous catalytic system, including stability, reusability, and easy recovery, is the functionalization of solid supports with organic molecules and active biomolecules⁷. Carbon-based nanomaterials are known as interesting solid support compounds, specifically two-dimensional nanosheet constituents, and their unique structure has led to charming physicochemical properties⁸. Among them, graphitic carbon nitride (g-C₃N₄) is recognized as a layered polymer whose attractive properties such as high stability, eco-friendly property, large surface area, rich in N, and nontoxicity have converted it into a valuable and useful class of carbon nanomaterials^{9,10}. Therefore, the widespread use of g-C₃N₄ sheets have been observed in various research fields consisting fuel cells, photoelectronic, water splitting, sensors, CO₂ reduction, solar energy conversion, and heterogeneous catalysis^{11–21}. However, applying functionalized g-C₃N₄ sheets in the catalytic field is an emerging topic; so, exploration of its new heterogeneous catalysts would be desirable and valuable. Several studies focused on the use of g-C₃N₄ for organic conversion, Mannich reaction, Knoevenagel condensation, reduction of N₂ to ammonia, and degradation of organic contaminations^{22–27}.

In particular, employing short and effective synthetic strategies can contribute to the development of green chemistry. Multicomponent reactions as a rapid synthesis strategy have concerned much attention as a green technique due to high atom economy, quick and easy performance, and saving time and energy²⁸. Numerous research studies have indicated that g-C₃N₄ is a sufficient support material for the implementation of multicomponent reactions. For example, Daraie et al. reported the activity of a heterogenous catalyst of silver incorporated into g-C₃N₄/Alginate in click coupling reactions²⁹. In another research effort, 1,2,3,6-tetrahydroquinazolines were

Department of Organic Chemistry, Faculty of Chemistry, University of Mazandaran, Babolsar, Iran. ✉ email: heshmat@umz.ac.ir; b.maleki@umz.ac.ir

synthesized through an efficient regioselective multicomponent synthesis in the presence of sulfonated $g\text{-C}_3\text{N}_4$ ³⁰. On the other hand, the tendency to reach an easy separable and rapid recyclable catalyst encouraged scientist to use magnetic/ $g\text{-C}_3\text{N}_4$. The nanocomposite of magnetic $g\text{-C}_3\text{N}_4$ was identified as an efficient catalyst for the one-pot multi-component synthesis of spirooxindoles³¹. In another research effort, a series of multicomponent tandem reactions were carried out by employing sulfonated $g\text{-C}_3\text{N}_4$ as a solid bifunctional catalyst³². Moradi et al. reported an effective synthesis of 2-amino-4*H*-chromene derivatives catalyzed by magnetic/silica/ $g\text{-C}_3\text{N}_4$ ³³.

Currently, magnetic nanoparticles (MNPs) support obtaining a beneficial separation by magnetic force that magnetic separation process is more facile than some traditional separation methods, such as filtration or high-speed centrifugation^{34,35}. However, to achieve more stable Fe_3O_4 NPs with diminished aggregation, surface modification was considered as an essential step in the catalyst preparation procedure. In addition, various natural, and synthesized polymer complexes coated with MNPs have been developed for high surface area, ease of preparation, more stable, userfriendly catalysts, and efficiency in a number of organic reactions^{36–38}.

Captopril (CAP) is a biodegradable and nontoxic molecule with thiol and carboxy acid groups that can act as a green efficient catalyst. Captopril is one of L-proline derivatives, biodegradable, and nontoxic molecule with pharmacological properties. It is a low-cost, green, and easily accessible ligand with thiol, and carboxy acid groups that has been used as an acidic, and efficient catalyst.³⁹ Herein, captopril was attached covalently on magnetic/ $g\text{-C}_3\text{N}_4$, and after characterization, the efficiency of this stable and reusable catalyst was investigated in the synthesis of two series of valuable heterocyclic compounds via one-pot multicomponent reaction processes. 2-amino-4*H*-chromene derivatives are known as anti-fungal, anti-cancer, and anti-bacterial agents; moreover, extensive industrial usage in photoactive compounds, agricultural chemicals, and pigments has stimulated researchers to study their synthesis methods^{40–42}. However, most of the published synthesis strategies suffer from some drawbacks, the need for high temperatures, long reaction times, and large amounts of catalyst^{43–46}. In this regard and to overcome these problems, in the field of catalyst and multicomponent synthesis reactions approaches, several derivatives of 2-amino-tetrahydro-4*H*-chromene-3-carbonitriles were synthesized in the presence of magnetic/ $g\text{-C}_3\text{N}_4$ /Cap.

The catalytic activity of the introduced catalyst was also investigated in the synthesis of 1,2,3,6-tetrahydropyrimidines via a one-pot three-component condensation reaction. Rare reports on the preparation of these heterocyclic compounds suffer from the serious disadvantage of by-product formation^{47–49}. To the best of our knowledge, successful efforts in the efficient synthesis of 1,2,3,6-tetrahydropyrimidines are limited to the use of a Zn-based catalytic system in this reaction⁵⁰. Accordingly, this work is in the vanguard in the metal-free synthesis of these biologically active compounds⁵¹.

Experimental

General

All chemicals were purchased from Merck and Sigma Aldrich and used without purification. Electro thermal 9100 apparatus was used to determine of melting points. Sonication for synthesis of catalyst was performed by Elma at 60 Hz. The FT-IR Spectra were detected through Shimadzu IR-470 spectrophotometer. Raman spectroscopy was carried out using a Takram P50C0R10 Raman system. The ¹H and ¹³C spectra of products were recorded with a Bruker DRX 400-Avance spectrometer. X-ray diffraction (XRD) pattern was recorded in Philips PW-1830. Magnetic analysis curves were attained by using VSM model MDKB from Danesh Pajohan Kavir Co. Kashan, Iran. The SEM images of the nanocatalyst were recorded via a MIRA₃ TESCAN-XMU instrument. TEM images were recorded with TEM Philips EM-208S, 100 kV. FEI TECNAI F20 instrument was applied for the achievement of high-resolution transmission electron microscopic (HRTEM) images. Elemental analysis of the nanocatalyst (EDS analysis) was done using TESCAN4992 instrument. Thermogravimetric analysis (TGA) was recorded by SDT Q600 V20.9 Build 20 instrument.

Preparation of $g\text{-C}_3\text{N}_4$ nanosheets

According to the reported method². The melamine was heated at 550 °C in a furnace at a ramp of 2.5 °C min⁻¹ in static air for 4 h so bulk $g\text{-C}_3\text{N}_4$ nanosheets powder was synthesized. Then bulk $g\text{-C}_3\text{N}_4$ (1.0 g) was treated in the mixture of 20.0 mL of HNO_3 and 20.0 mL of H_2SO_4 at room temperature for 2 h. The mixture was diluted with 1.0 L of deionized H_2O , and the obtained precipitate was filtered and washed several times with deionized water and dried at 60 °C. Then, treated bulk $g\text{-C}_3\text{N}_4$ (1.0 g) was dispersed in 100.0 mL of water/isopropanol (1:1) by sonication for approximately 6 h. Finally, to separate the residual unexfoliated $g\text{-C}_3\text{N}_4$ nanoparticles, the formed suspension was centrifuged (5000 rpm).

Synthesis of $\text{Fe}_3\text{O}_4@g\text{-C}_3\text{N}_4$

Magnetic graphite-like graphitic carbon nitride ($g\text{-C}_3\text{N}_4$) was prepared through known reported method⁵². Initially, graphitic carbon nitride (0.4 g) was dispersed in 50 ml deionized water (DI) for 4 h in ultrasonic conditions; then $\text{FeCl}_3\cdot 6\text{H}_2\text{O}$ (4.68 g, 17.3 mmol) and $\text{FeCl}_2\cdot 4\text{H}_2\text{O}$ (2.3 g, 18.14 mmol) were added to the solution. Then, aqueous ammonia solution (15 ml, 25%) was added drop wise to the previous mixture until the pH reached 9–10. The mixture was stirred at 80 °C for 2 h under nitrogen atmosphere. The resulting black solid was separated by an external magnet and washed thoroughly with DI water and absolute ethanol, then dried at 50 °C for overnight to provide the $\text{Fe}_3\text{O}_4@g\text{-C}_3\text{N}_4$.

Synthesis of $\text{Fe}_3\text{O}_4@g\text{-C}_3\text{N}_4\text{-PrBr}$

The resulting $\text{Fe}_3\text{O}_4@g\text{-C}_3\text{N}_4$ (0.5 g) were dispersed in 15.0 mL of dry toluene in ultrasonic conditions then, 1,3-dibromopropane (10 mmol, 1.1 mL) and sodium iodide (0.5 mmol, 0.075 g) was added to the dispersed solution, and the reaction mixture was refluxed overnight under inert atmosphere. The resulted mixture was

cooled to room temperature and obtained brown solid was collected by using an external magnet bar, washed with ethyl acetate, and dried at room temperature overnight.

Synthesis of $\text{Fe}_3\text{O}_4@g\text{-C}_3\text{N}_4\text{-Pr-Cap}$

$\text{Fe}_3\text{O}_4@g\text{-C}_3\text{N}_4\text{-PrBr}$ (0.5 g) was added into a round bottom flask containing 15 mL of dry toluene and dispersed under ultrasonic conditions for 30 min. Then, sodium iodide (0.5 mmol, 0.075 g) and captopril (0.5 mmol, 0.11 g) were added into the mixture under reflux in toluene (110 °C) for 48 h, under inert atmosphere. The mixture was cooled to room temperature and the catalyst was separated magnetically and washed with absolute ethanol, and subsequently dried at room temperature for 12 h.

General procedure for the one-pot synthesis of 2-amino-4H-chromene derivatives

Benzaldehydes (1.0 mmol), malononitrile or ethyl cyanoacetate (1.0 mmol), and *CH*- or *OH*-acids (1.0 mmol) were added in 3 mL of ethanol in presence of 20 mg of the catalyst. This mixture stirred for appropriate times at 50 °C. The progress of the reaction was monitored by TLC (ethyl acetate: n-hexane, 1:1). After completion of the reaction, the catalyst was separated using an external magnet bar, the reaction mixture was diluted with diethyl ether (15 mL) and dried with anhydrous MgSO_4 . Then the mixture was filtered and washed with diethyl ether and purified via recrystallization in ethanol to reach pure products.

General procedure for the one-pot synthesis of 1,2,3,6-tetrahydropyrimidine

Benzaldehydes (1.2 mmol), EtOH (3 mL), and catalyst (20 mg) were added successively to a stirring mixture of diethyl acetylene dicarboxylate (1.0 mmol) and anilines (2.0 mmol). The mixture was stirred at 50 °C for appropriate times. The reaction progress was monitored by TLC. After completion of the reaction, the catalyst was separated, the reaction mixture was diluted with diethyl ether (15 mL) and dried with anhydrous MgSO_4 . Then the mixture was filtered and washed with diethyl ether and the product was purified through recrystallization in ethanol to reach pure products.

Results and discussion

The schematic of catalyst preparation has been illustrated in (Fig. 1) to prepare the $\text{Fe}_3\text{O}_4@g\text{-C}_3\text{N}_4$ nanoparticles, iron salts were added to $g\text{-C}_3\text{N}_4$ prepared from the thermal polymerization of melamine and liquid exfoliation process in flowing (Fig. 1). The presence of functional groups on the $\text{Fe}_3\text{O}_4@g\text{-C}_3\text{N}_4$, its surface was functionalized with 1,3-dibromopropane as a functionalizing agent to prepare $\text{Fe}_3\text{O}_4@g\text{-C}_3\text{N}_4\text{-PrBr}$. The immobilization of the captopril contains the carboxylic acid group on the magnetic graphitic carbon nitride for the first time is the main novelty of this work ($\text{Fe}_3\text{O}_4@g\text{-C}_3\text{N}_4\text{-Pr-Cap}$) as acidic nanocatalyst.

The FT-IR spectroscopy was employed to characterize the synthesized particles and their modifications. In the spectrum of $\text{Fe}_3\text{O}_4@g\text{-C}_3\text{N}_4$ (Fig. 2a), a broad and strong peak of N–H group and O–H appeared around 2800–3600 cm^{-1} , stretching vibration peaks of C=N were observed at 1637 and 1571 cm^{-1} , stretching peaks of the C–N heterocycle were at around 1461, 1322, and 1241 cm^{-1} , and a sharp peak at 810 cm^{-1} is due to the breathing vibration of tri-s-triazine units. The presence of a strong band at 565–632 cm^{-1} is related to the Fe–O band in the MNPs. The chemical structure of this intermediate compound, $\text{Fe}_3\text{O}_4@g\text{-C}_3\text{N}_4\text{-PrBr}$, was also confirmed by FT-IR (Fig. 2b). Observation of the main adsorption bands of $g\text{-C}_3\text{N}_4$ indicating the presence of basic $g\text{-C}_3\text{N}_4$ chemical structure. The spectrum of the final composite, $\text{Fe}_3\text{O}_4@g\text{-C}_3\text{N}_4\text{-Pr-Cap}$, is given in (Fig. 2c), the presence of 1690 cm^{-1} and 1307 cm^{-1} peaks of C=O and C–O bonds, respectively; approves the existence of captopril in the catalyst. The spectra of modified $g\text{-C}_3\text{N}_4$ also presented O–H and C–H bonds in the structure.

The preparation of the intermediate compound, $\text{Fe}_3\text{O}_4@g\text{-C}_3\text{N}_4\text{-PrBr}$, and the final composite, $\text{Fe}_3\text{O}_4@g\text{-C}_3\text{N}_4\text{-Pr-Cap}$, was also approved by EDS. The EDS spectrum shows the composition of Br atoms in the framework (Fig. 3a) indicating linker attaches to magnetic graphitic carbon nitride. The EDS spectra of the final composite have also been depicted in (Fig. 3b), the existence of the constituent elements of this compound confirmed the formation.

Raman was used to further illustrate the chemical structure of the $\text{Fe}_3\text{O}_4@g\text{-C}_3\text{N}_4$ nanocomposites (Fig. 4). $\text{Fe}_3\text{O}_4@g\text{-C}_3\text{N}_4\text{-Pr-Cap}$ showed two main Raman bands at 223 and 652 cm^{-1} corresponding to vibrational modes of magnetite Fe_3O_4 . In the Raman pattern of $g\text{-C}_3\text{N}_4$, 704 cm^{-1} was the typical 3-s-triazine ring breathing vibrational mode peak. Peak at 1325 cm^{-1} represented the D-band, and peak at 1583 cm^{-1} represented the G-band. Peak at 1624 and 1696 cm^{-1} , indicating the presence of C=O groups of the captopril.

FE-SEM, TEM, and HR-TEM analysis were applied to study the surface morphology of the catalyst, nano size, uniform distribution, and spherical shape of the particles have been illustrated in (Figs. 5, 6, and 7). Accordingly, the average diameter of nanoparticles was found less than 30 nm. The FE-SEM images obtained indicated wrinkled lamellar structure with relatively smooth surface, suggesting that the surface of $\text{Fe}_3\text{O}_4@g\text{-C}_3\text{N}_4$ sheets were immobilized with captopril.

The thermal behaviour of the prepared composite was investigated using thermogravimetric analysis, and decomposition cures of the final composite and its precursor have been depicted in (Fig. 8). The first weight loss step blew 200 °C, attributed to solvent and water releasing in all samples. The second step of weight loss in the range of 200–597 °C comes from the decomposition of organic groups of structures. The thermal stability of the synthesized composite was confirmed by low weight loss at higher temperatures.

The elemental analysis and the percent of weight loss in TGA results were used to calculate the amount of loaded organic species. Captopril is just a source of S in the synthesized composite; therefore, the amount of S (5.08 mmol g^{-1} , from elemental analysis) was used to find captopril loaded amount (0.75 mmol g^{-1}) in harmony with TGA results (0.78 mmol g^{-1}).

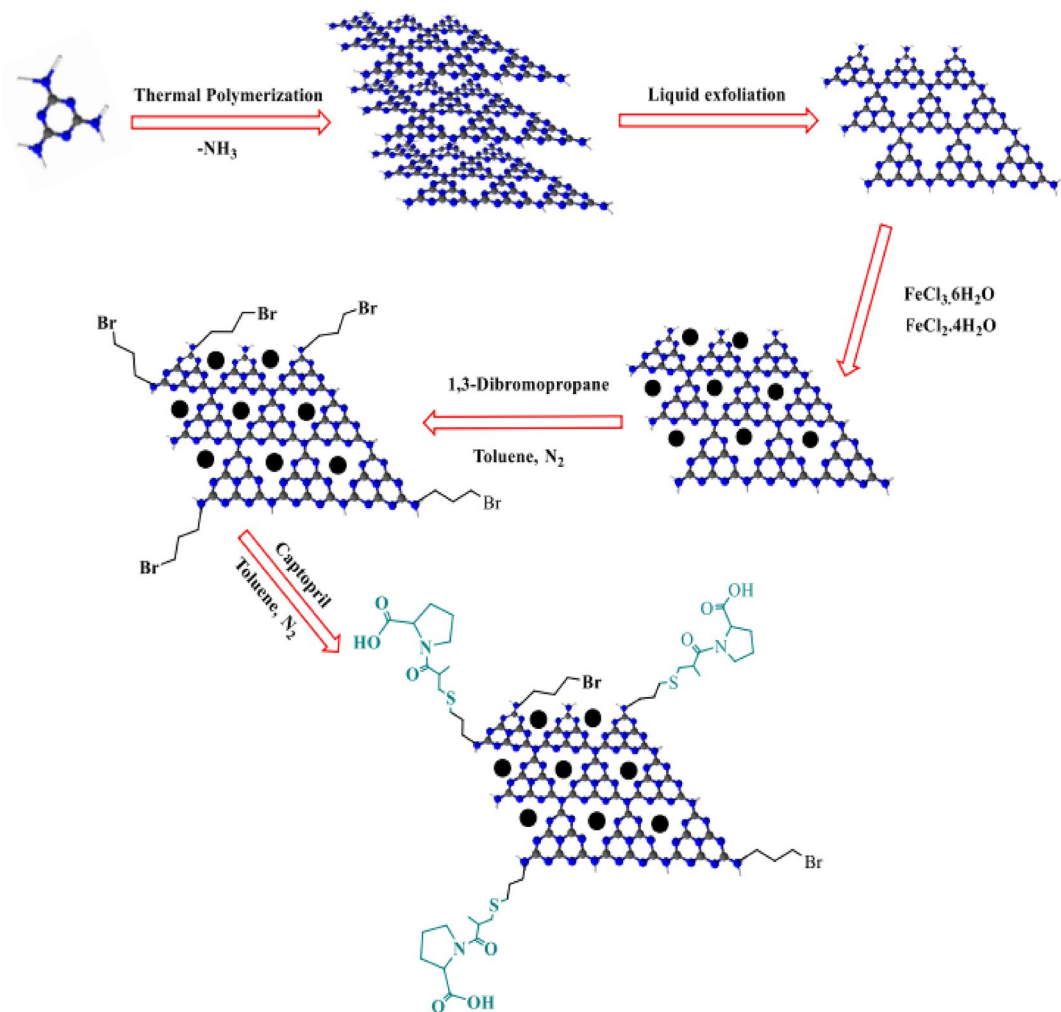


Figure 1. Preparation schematic of $\text{Fe}_3\text{O}_4@\text{g-C}_3\text{N}_4\text{-Pr-Cap}$.

The magnetic properties of $\text{Fe}_3\text{O}_4@\text{g-C}_3\text{N}_4$ and the catalyst were investigated and the values were found as 19.25 emu g^{-1} and 14.89 emu g^{-1} , respectively; their related curves are depicted in (Fig. 9). This paramagnetic activity of the catalyst was found to be lower than $\text{Fe}_3\text{O}_4@\text{g-C}_3\text{N}_4$ which may be related to the coating of magnetic graphene nitride with captopril.

The XRD spectrum of the catalyst and its precursor has been presented in (Fig. 10), distinguishing diffraction peaks at $2\theta = 30.4^\circ, 35.6^\circ, 44.4^\circ, 57.4^\circ, 63.1^\circ,$ and 74.6° are related to Fe_3O_4 nanoparticles with cubic phase. Moreover, the presence of conjugated aromatic systems with interplanar stacking corresponding to units $\text{g-C}_3\text{N}_4$ was depicted by existence of diffraction peaks at $2\theta = 27.3^\circ$.

After synthesis and characterization of the final composite, its catalytic efficiency was investigated in MCR for 2-amino-4H-chromenes synthesis. Initially, the MCR of benzaldehyde, malononitrile, and dimedone was selected as a model for reaction conditions optimization, including the study of the influence of catalyst amount, the kind of solvent, and reaction temperature on reaction performance. The outcomes are listed in Table 1.

For screening of the catalysts, the reaction was performed in ethanol at 80°C , without any catalyst, and in the presence of pure magnetic nanoparticles, the reaction was intact (Table 1, entries 1, 4). Employing $\text{Fe}_3\text{O}_4@\text{g-C}_3\text{N}_4$ and $\text{Fe}_3\text{O}_4@\text{g-C}_3\text{N}_4\text{-PrBr}$ afforded negligible conversion (Table 1, entries 2, 3). Pure captopril, safe, easily accessible, and low-cost organic compound, exhibited significant efficiency in model reaction (Table 1, entry 5) approved its property; however, considering green chemistry supporting from easy recyclable bed to generation of heterogenous catalyst is a more desirable approach. Interestingly, the magnetic nanoparticle-supported captopril was shown excellent activity in the intended reaction (Table 1, entry 6). After screening the catalyst, the effect of catalyst amount was investigated, more amount of catalysts didn't give better results (Table 1, entry 7), and lower amounts of catalyst gave weak performance (Table 1, entry 8).

Through the advance of green chemistry, using green media in chemical reactions has been converted into an attractive target in scientific efforts. In this regard, in comparison with flammable and volatile organic solvents, DMF, MeOH, and EtOH are considered safe solvents (Table 1, entries 9, 10). However, among them, EtOH was recognized as a more economical, ecological, and versatile solvent that created suitable reaction conditions to achieve excellent performance, but the application of water and solvent-free media was not succeeded (Table 1,

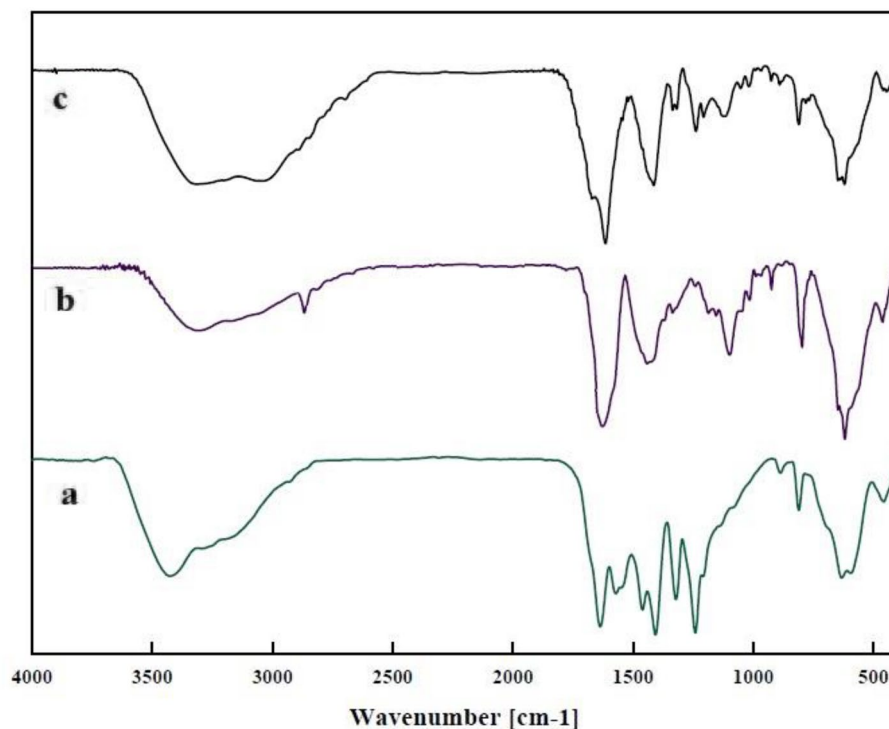


Figure 2. The FT-IR spectra of (a) $\text{Fe}_3\text{O}_4@g\text{-C}_3\text{N}_4$, (b) $\text{Fe}_3\text{O}_4@g\text{-C}_3\text{N}_4\text{-PrBr}$, (c) $\text{Fe}_3\text{O}_4@g\text{-C}_3\text{N}_4\text{-Pr-Cap}$.

entries 11, 12). Low-temperature reactions are considered a green strategy due to cost-effectiveness, less energy consumption, and less chance of byproduct formation. The reaction was performed in milder conditions (Table 1, entry 13). Paying attention to the reaction time reached out to this conclusion that the reaction was completed in less time (Table 1, entry 15).

Optimization reaction conditions in hands, the generality of the catalyst was investigated through the synthesis of several derivatives. The chemical structure of processors, products, and reaction results have been presented in Table 2. Employing several derivatives of benzaldehyde, other components of the reaction keeping the same (Table 2, entries 1–12), with different electronic natures indicating that their electronic properties are not very important points in this reaction, resulting in high reaction yields and short reaction time for all cases. However, replacing dimedone with other diketones led to longer reaction times (Table 2, entries 13–19). As shown in Table 2, in all cases, the products were formed in high to excellent yields (89–97%). In general, our sustainable catalytic system was found as a very active and efficient catalyst for the synthesis of a series of heterocyclic compounds. A gram scale 2-amino-4*H*-chromene reaction was carried out using optimized reaction conditions. The 2-amino-4*H*-chromene reaction (Table 2, entry 5) of benzaldehyde (1.6 g, 15 mmol), malononitrile (1.0 g, 15 mmol), and dimedone (2.1 g, 15 mmol), in presence of EtOH (45 mL) using 0.3 g of the catalyst at 50 °C was conducted. When the scale of the reaction was increased to 15 mmol, the reaction was still found to proceed successfully and the corresponding product was obtained in 90% yield.

The proposed mechanism of the 2-amino-4*H*-chromene synthesis in the presence of $\text{Fe}_3\text{O}_4@g\text{-C}_3\text{N}_4\text{-Pr-Cap}$ has been depicted in (Fig. 11). Captopril supported on magnetic graphene nitride has several acidic catalytic active sites which activate benzaldehyde. Then, malononitrile reacted with the active carbonyl of benzaldehyde, Knoevenagel condensation, Michael addition, and final cyclization leading to the final product.

As a comparison study, the activity of $\text{Fe}_3\text{O}_4@g\text{-C}_3\text{N}_4\text{-Pr-Cap}$ has been compared with reported catalytic systems applied for the one-pot multicomponent reaction for 2-amino-4*H*-chromenes synthesis. The results are listed in Table 3, as can be seen, our catalytic system illustrated high efficiency at extremely short reaction time in desirable mild reaction conditions.

Encouraged by excellent outcomes of 2-amino-4*H*-chromenes synthesis investigation and optimization reaction conditions in hands (Cat. 20 mg, EtOH (3 mL), 50 °C) of the 1,2,3,6-tetrahydropyrimidine derivatives synthesis was performed. Benzaldehydes with diverse electronic properties substituted competently with anilines and diethyl acetylenedicarboxylate, and high yields of products were attained (Table 4). Accordingly, starting materials with different electronic natures did not exhibited any important effect on the reaction yields.

A plausible mechanism of 1,2,3,6-tetrahydropyrimidine synthesis has been given in (Fig. 12). Hydroamination occurred in the first step and amidation was performed in the next step by acid activation assistance. The product was formed in the last step through aldehyde dehydration and cyclization processes.

Difficult separation of homogeneous catalysts is known as a serious problem in chemical transportation due to their economic and environmental disadvantages. In this work, a heterogeneous magnetic catalyst was introduced, and after an investigation of its efficiency, its recyclability was studied. For this purpose, after the

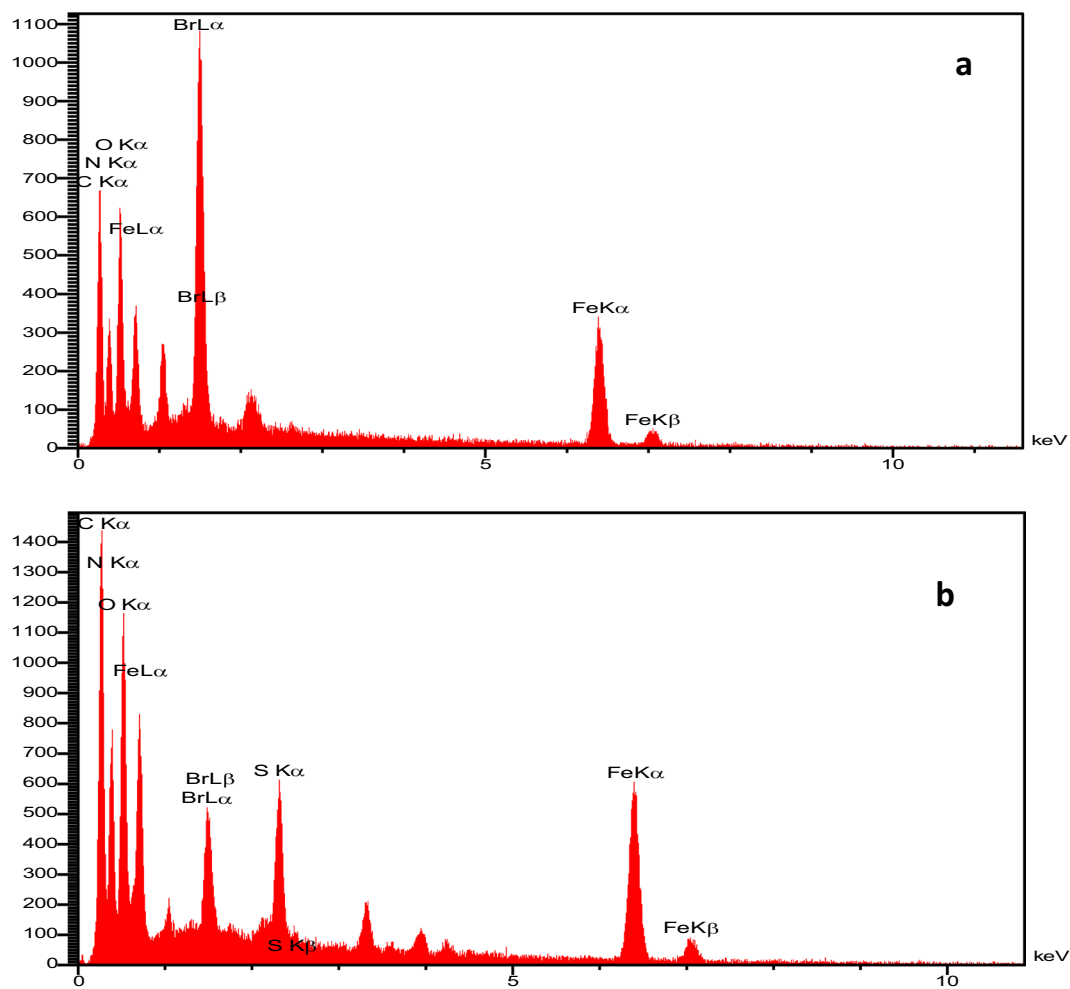


Figure 3. EDS spectra of $\text{Fe}_3\text{O}_4@g\text{-C}_3\text{N}_4\text{-PrBr}$ (a), $\text{Fe}_3\text{O}_4@g\text{-C}_3\text{N}_4\text{-Pr-Cap}$ (b).

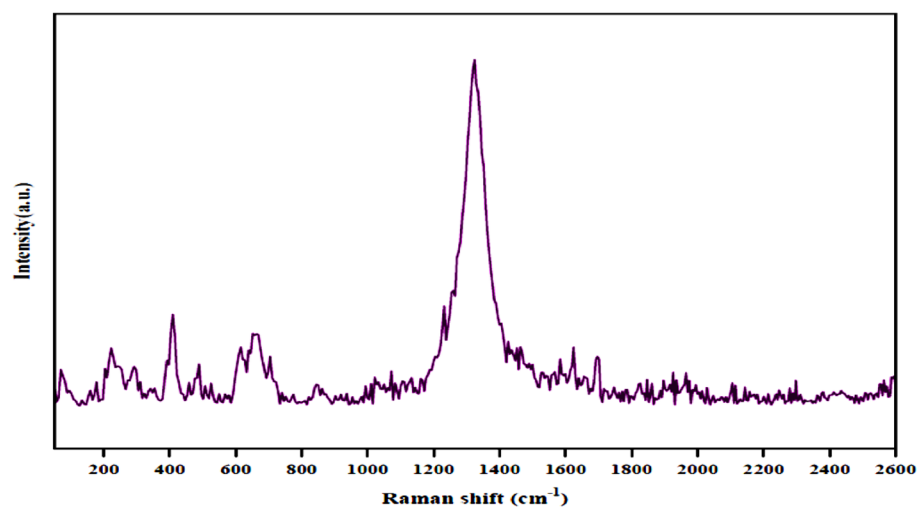


Figure 4. Raman spectra of $\text{Fe}_3\text{O}_4@g\text{-C}_3\text{N}_4\text{-Pr-Cap}$.

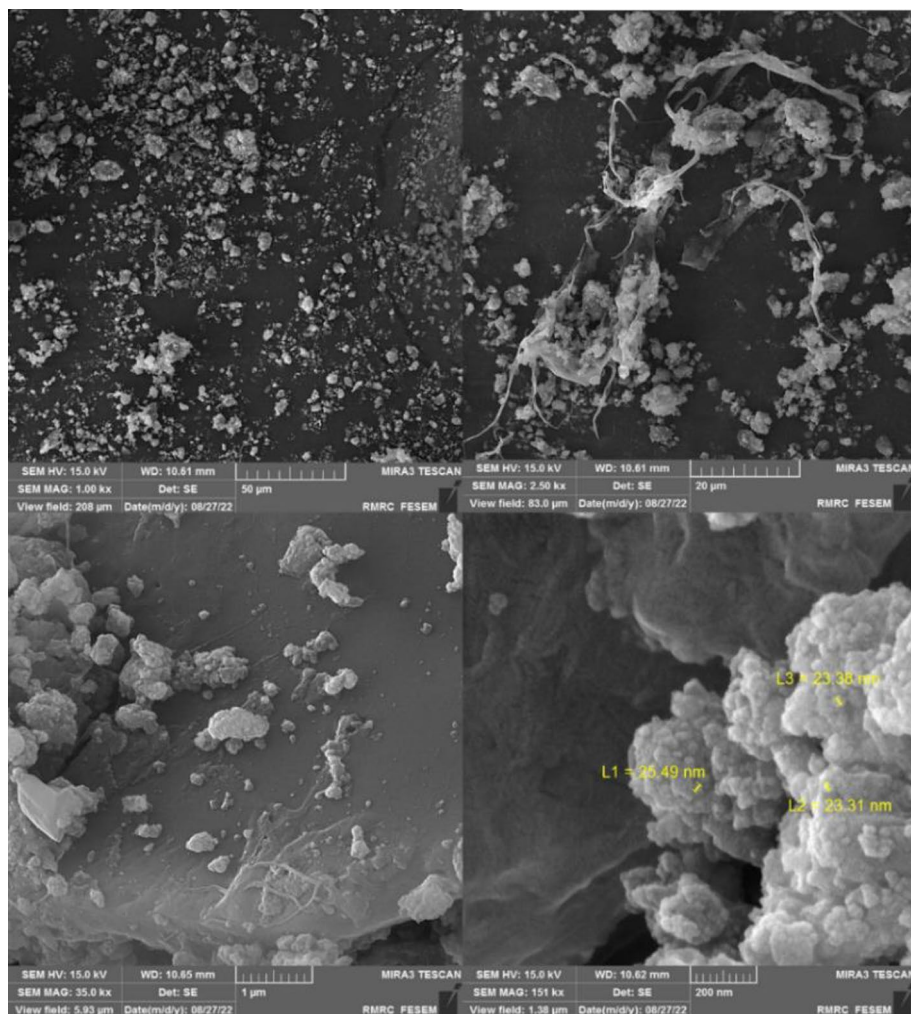


Figure 5. FE-SEM images of $\text{Fe}_3\text{O}_4@g\text{-C}_3\text{N}_4\text{-Pr-Cap}$.

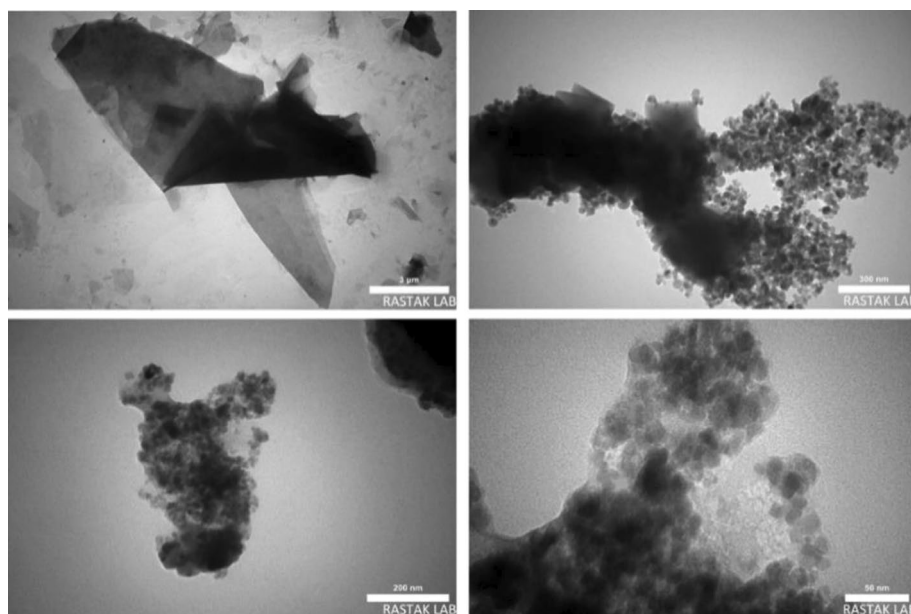


Figure 6. TEM images of $\text{Fe}_3\text{O}_4@g\text{-C}_3\text{N}_4\text{-Pr-Cap}$.

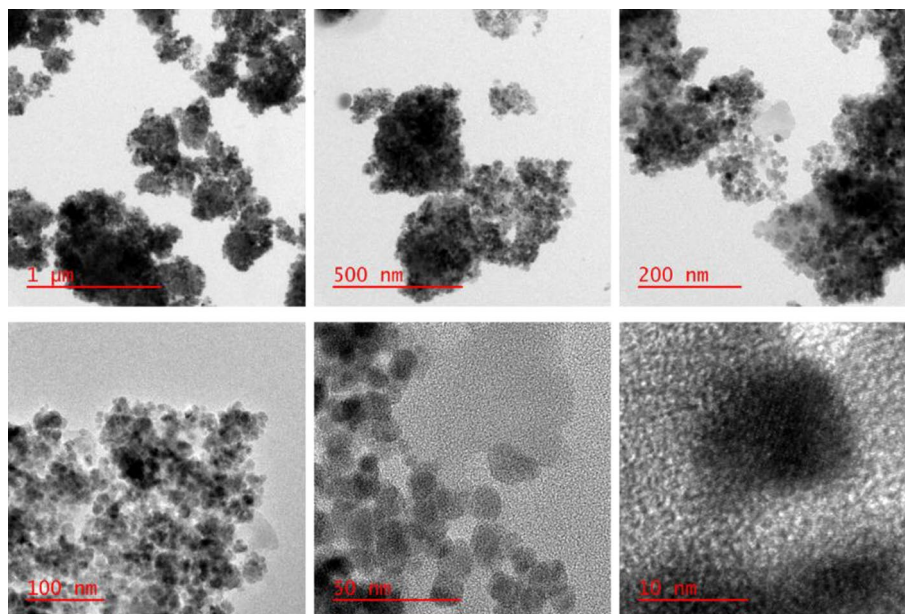


Figure 7. HR-TEM images of $\text{Fe}_3\text{O}_4@\text{g-C}_3\text{N}_4\text{-Pr-Cap}$.

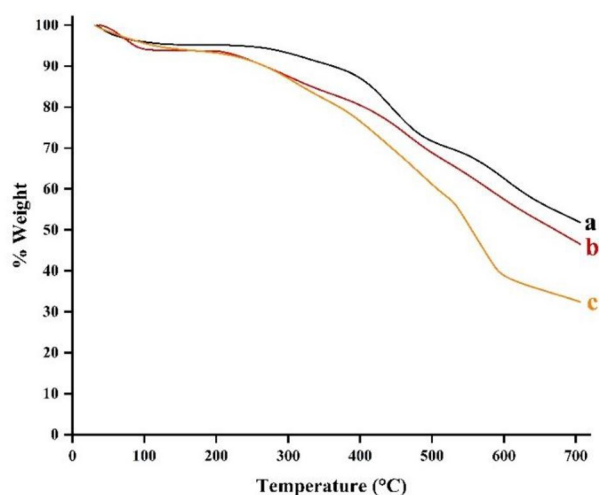


Figure 8. TGA plots of $\text{Fe}_3\text{O}_4@\text{g-C}_3\text{N}_4$ (a), $\text{Fe}_3\text{O}_4@\text{g-C}_3\text{N}_4\text{-PrBr-Cap}$ (b), $\text{Fe}_3\text{O}_4@\text{g-C}_3\text{N}_4\text{-Pr-Cap}$ (c).

reaction completion, separation of the catalyst from the reaction mixture was done by employing an external magnet bar, washed, and reused in another fresh reaction mixture. The performance of reused catalysts for both studied reactions has been reported in (Fig. 13). The catalyst exhibited significant activity even after five times using. The recycled catalyst was characterized through several analysis methods including XRD, and SEM. The results are reported in (Figs. 14 and 15), these results indicated that no significant changes were observed in comparison with fresh catalyst.

Based on the use of captopril on the catalyst surface and its acidic groups, it leads to spatial congestion with other molecules on the catalyst surface. This spatial congestion can result in the closure of the proximity space around the C–Br bond. It can hinder the interaction of the C–Br bond with other molecules in the reactants, thereby reducing its role. When the catalyst surface is filled with adsorbent groups, the free space for molecular interactions decreases. This can cause congestion and a reduction in interactions involving a specific bond in the reactant molecules. As a result, interactions that rely on that bond for catalytic activity decrease, leading to a diminished role of the C–Br bond in the reaction. Ultimately, the reactive components interact with the free acidic groups in the structure of captopril, promoting reaction progress and high product yield. However, if the reactive components were to react with C–Br instead, it would not result in high product yields. Refer to Tables 2 and 4 to see the yield of the products. In addition to this, the recovered catalyst ($\text{Fe}_3\text{O}_4@\text{g-C}_3\text{N}_4\text{-Pr-Cap}$) was characterized by Energy-dispersive X-ray spectroscopy (EDS) and FT-IR (Figs. 16, and 17). The EDS spectrum displays the

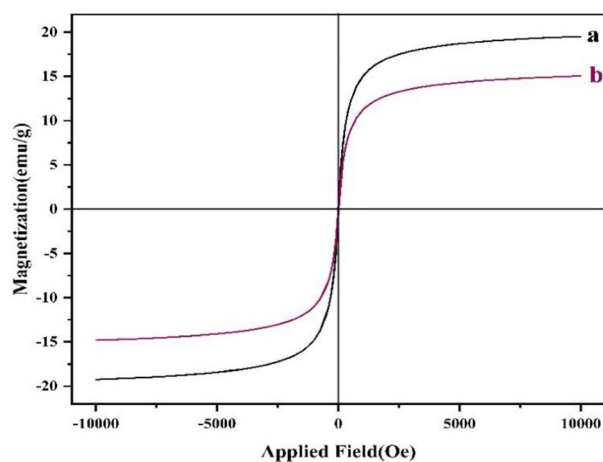


Figure 9. Magnetization curves of $\text{Fe}_3\text{O}_4@g\text{-C}_3\text{N}_4$ (a), $\text{Fe}_3\text{O}_4@g\text{-C}_3\text{N}_4\text{-Pr-Cap}$ (b).

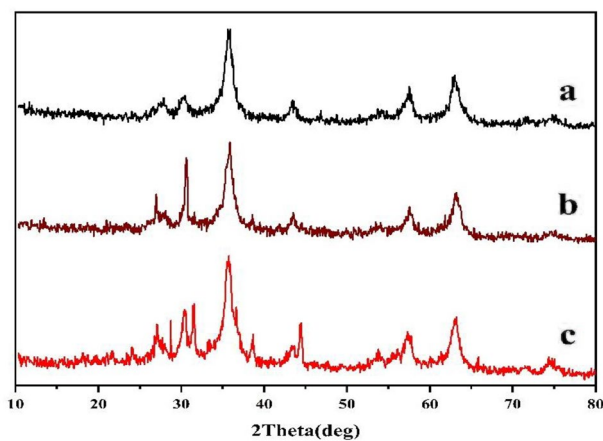
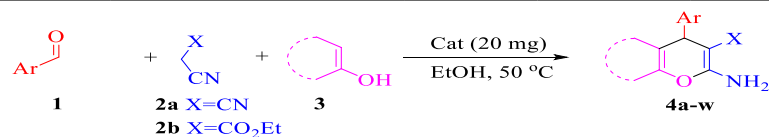


Figure 10. $\text{Fe}_3\text{O}_4@g\text{-C}_3\text{N}_4$ (a), $\text{Fe}_3\text{O}_4@g\text{-C}_3\text{N}_4\text{-PrBr-Cap}$ (b), $\text{Fe}_3\text{O}_4@g\text{-C}_3\text{N}_4\text{-Pr-Cap}$ (c).

Entry	Solvent	Catalyst (mg)	t (min)	T (°C)	Yield ^b (%)
1	EtOH	–	30	80	–
2	EtOH	$\text{Fe}_3\text{O}_4@g\text{-C}_3\text{N}_4$ (20)	30	80	28
3	EtOH	$\text{Fe}_3\text{O}_4@g\text{-C}_3\text{N}_4\text{-PrBr}$ (20)	30	80	32
4	EtOH	Fe_3O_4 (20)	30	80	Trace
5	EtOH	Captopril (20)	30	80	97
6	EtOH	$\text{Fe}_3\text{O}_4@g\text{-C}_3\text{N}_4\text{-Pr-Cap}$ (20)	30	80	95
7	EtOH	$\text{Fe}_3\text{O}_4@g\text{-C}_3\text{N}_4\text{-Pr-Cap}$ (30)	30	80	95
8	EtOH	$\text{Fe}_3\text{O}_4@g\text{-C}_3\text{N}_4\text{-Pr-Cap}$ (10)	30	80	83
9	MeOH	$\text{Fe}_3\text{O}_4@g\text{-C}_3\text{N}_4\text{-Pr-Cap}$ (20)	30	80	86
10	DMF	$\text{Fe}_3\text{O}_4@g\text{-C}_3\text{N}_4\text{-Pr-Cap}$ (20)	30	80	73
11	H ₂ O	$\text{Fe}_3\text{O}_4@g\text{-C}_3\text{N}_4\text{-Pr-Cap}$ (20)	30	80	80
12	Solvent free	$\text{Fe}_3\text{O}_4@g\text{-C}_3\text{N}_4\text{-Pr-Cap}$ (20)	30	80	44
13	EtOH	$\text{Fe}_3\text{O}_4@g\text{-C}_3\text{N}_4\text{-Pr-Cap}$ (20)	30	50	95
14	EtOH	$\text{Fe}_3\text{O}_4@g\text{-C}_3\text{N}_4\text{-Pr-Cap}$ (20)	30	25	82
15	EtOH	$\text{Fe}_3\text{O}_4@g\text{-C}_3\text{N}_4\text{-Pr-Cap}$ (20)	15	50	95

Table 1. Optimization for Synthesis of 2-amino-4*H*-chromene^a. ^aReaction conditions: benzaldehyde (1.0 mmol), malononitrile (1.0 mmol), dimedone (1.0 mmol), and solvent (3.0 ml). ^bIsolated yield.



Entry	R	X	CH- or OH- acids 3	Products	Time (min)	Yield ^b (%)	Mp (°C)	
							Observed	Literature
1	4-CN-C ₆ H ₄	CN	Dimedone	4a	3	94	228–230	229–231 ⁵³
2	4-NO ₂ -C ₆ H ₄	CN	Dimedone	4b	2	97	175–178	176–183 ⁵⁴
3	4-CHO-C ₆ H ₄	CN	Dimedone	4c	5	96	271–273	273–275 ⁵⁵
4	4-Cl-C ₆ H ₄	CN	Dimedone	4d	3	97	212–215	214–216 ⁵⁴
5	C ₆ H ₅	CN	Dimedone	4e	4	95	258–261	257–259 ⁵⁴
6	4-OH-C ₆ H ₄	CN	Dimedone	4f	4	92	224–227	224–226 ⁵³
7	4-NMe ₂ -C ₆ H ₄	CN	Dimedone	4g	4	93	211–213	209–210 ⁵⁴
8	Furan-2-yl	CN	Dimedone	4h	10	91	224–226	221–222 ⁵⁶
9	Thiophene-2-yl	CN	Dimedone	4i	10	86	213–215	210–212 ⁵⁷
10	4-CN-C ₆ H ₄	CO ₂ Et	Dimedone	4j	4	92	179–182	181–183 ⁵⁶
11	4-NO ₂ -C ₆ H ₄	CO ₂ Et	Dimedone	4k	5	91	152–154	153–154 ⁵⁸
12	4-Cl-C ₆ H ₄	CO ₂ Et	Dimedone	4l	5	94	153–155	153–156 ⁵⁸
13	C ₆ H ₅	CO ₂ Et	Dimedone	4m	7	93	149–152	148–150 ⁵⁸
14	4-NMe ₂ -C ₆ H ₄	CO ₂ Et	Dimedone	4n	7	93	155–157	156–157 ⁵⁹
15	4-Cl-C ₆ H ₄	CN	Ethyl acetoacetate	4o	12	90	171–173	172–174 ⁶⁰
16	4-Cl-C ₆ H ₄	CN	6-Methyl-2H-pyran-2,4(3H)-dione	4p	15	95	230–234	230–232 ⁵³
17	4-Cl-C ₆ H ₄	CN	Barbituric acid	4q	12	94	233–236	234–236 ⁵³
18	4-Cl-C ₆ H ₄	CN	3-Methyl-4H-pyrazole-5(4H)-one	4r	15	89	232–234	234–236 ⁶⁰
19	4-Cl-C ₆ H ₄	CN	1,3-Indandione	4s	15	97	288–291	287–289 ⁶¹
20	4-Cl-C ₆ H ₄	CN	4-Hydroxycoumarin	4t	10	95	264–266	263–265 ⁵³
21	4-Cl-C ₆ H ₄	CN	2-Naphthol	4v	15	93	206–209	205–206 ⁶²
22	Furan-2-yl	CN	2-Naphthol	4u	15	88	220–223	220–222 ⁵⁶
23	Thiophene-2-yl	CN	2-Naphthol	4w	15	85	260–260	258–259 ⁵⁶

Table 2. Synthesis of 2-amino-4H-chromene derivatives using the catalyst^a. ^aReaction carried out with benzaldehydes (1.0 mmol), malononitrile or ethyl cyanoacetate (1.0 mmol) and Diketone (1.0 mmol) in a 3.0 mL EtOH using 20 mg of the catalyst at 50 °C. ^bIsolated yield. ^cReaction carried out with terephthalaldehyde (1.0 mmol), malononitrile (2.0 mmol) and dimedone (2.0 mmol), in 3.0 mL EtOH using 20 mg of the catalyst at 50 °C.

presence of Br atoms without significant change in comparison with fresh catalyst (Fig. 3b), which is a confirmation that the C–Br bond remains unchanged. The FT-IR of the fresh and recycled catalyst, Fe₃O₄@g-C₃N₄-Pr-Cap, is given in (Fig. 17). In Fig. 17b, the presence of stretching and bending vibrations of the C–Br at 700 cm⁻¹ and 1100 cm⁻¹, respectively; approves that C–Br bond remains unchanged.

Conclusion

A magnetically recoverable and green catalyst was developed by immobilizing a safe and sustainable ligand on magnetic graphene nitride. The chemical nature and properties of the catalyst were characterized by different analysis techniques. From the values and the importance of the one-pot multicomponent reaction for the synthesis of heterocycles, we discovered that our environmentally friendly and sustainable catalytic system was super active for the synthesis of a wide-scope of 2-amino-4H-chromenes and 1,2,3,6-tetrahydropyrimidine under mild and green conditions. Moreover, the common problem in these reactions is the formation of unwanted byproducts, which were not formed in the presented synthesis method. The Fe center of the catalyst makes it attractive due to the low cost, availability, and low toxicity of this metal. Magnetic core led to an easy recyclability process; moreover, the catalyst exhibited excellent reusability in at least five reaction runs.

Ethical approval

This work does not contain any studies with human participants or animals performed by any of the authors.

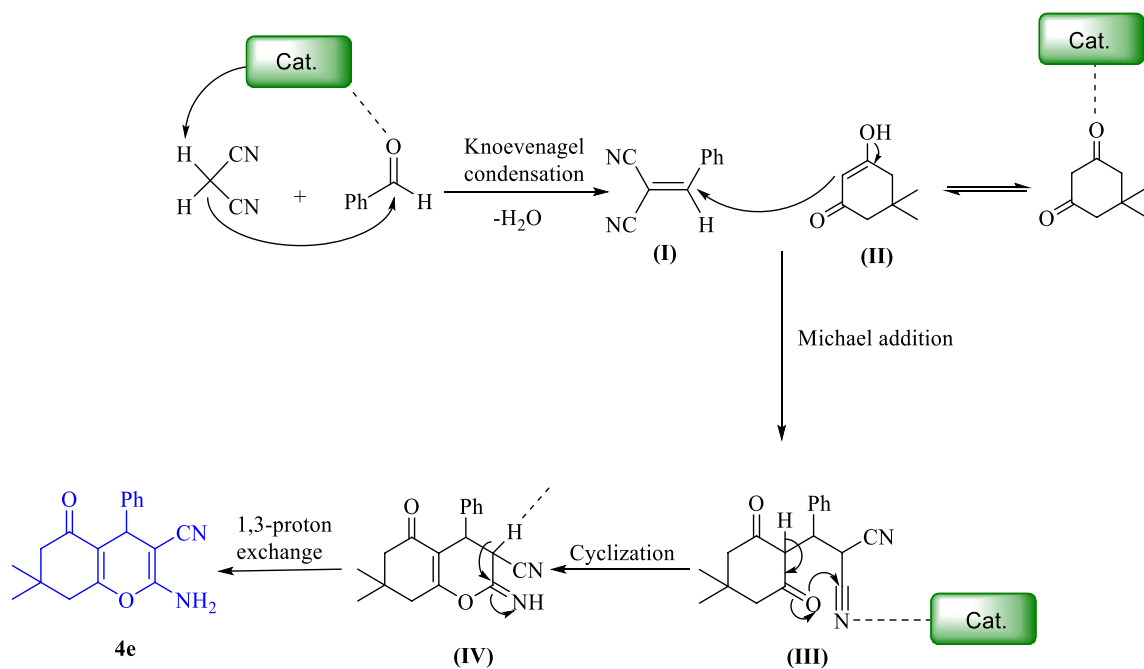
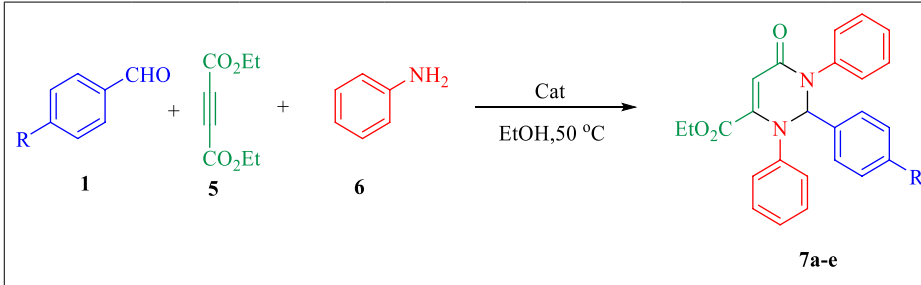


Figure 11. Proposed mechanism 2-amino-4H-chromenes synthesis in the presence of the catalyst.

Entry	Catalyst (mg)	Solvent	Time (min)	Yield % ^a	References
1	Melamine	H ₂ O/EtOH	25	93	63
2	Aminopropylated silica gel	H ₂ O	90	89	64
3	CuFe ₂ O ₄ @strach	EtOH	20	96	65
4	Fe ₃ O ₄ @MCM-41@Zr-piperazine	H ₂ O/EtOH	30	85	66
5	2-Aminopyrine	EtOH	8	92	67
6	MNPs-GO-CysA	H ₂ O/EtOH	15	93	68
7	Fe ₃ O ₄ @SiO ₂ -creatine	EtOH	6	94	43
8	Fe ₃ O ₄ @g-C ₃ N ₄ -Pr-Cap	EtOH	3	96	This work

Table 3. Comparison of our catalyst with previous reported catalysts^a. ^aAll reactions were performed employing 4-chlorobenzaldehyde (1.0 mmol), malononitrile (1.1 mmol) and dimesone (1.0 mmol).



Entry	R	Products	Time (h)	Yield ^b (%)	Mp (°C)	
					Observed	Literature
1	NO ₂	7a	8	86	169–171	–
2	F	7b	8	79	175–178	176–183 ⁵⁰
3	Br	7c	8	69	162–165	164–166 ⁵⁰
4	H	7d	8	80	167–169	166–169 ⁵⁰
5	Me	7e	8	83	151–154	150–153 ⁵⁰

Table 4. Synthesis of 1,2,3,6-tetrahydropyrimidine derivatives using the catalyst^a. ^aReaction carried out with anilines (2.0 mmol), diethyl acetylenedicarboxylate (1.0 mmol) and benzaldehydes (1.2 mmol), in a 3.0 mL EtOH using 20 mg of the catalyst at 50 °C. ^bIsolated yield.

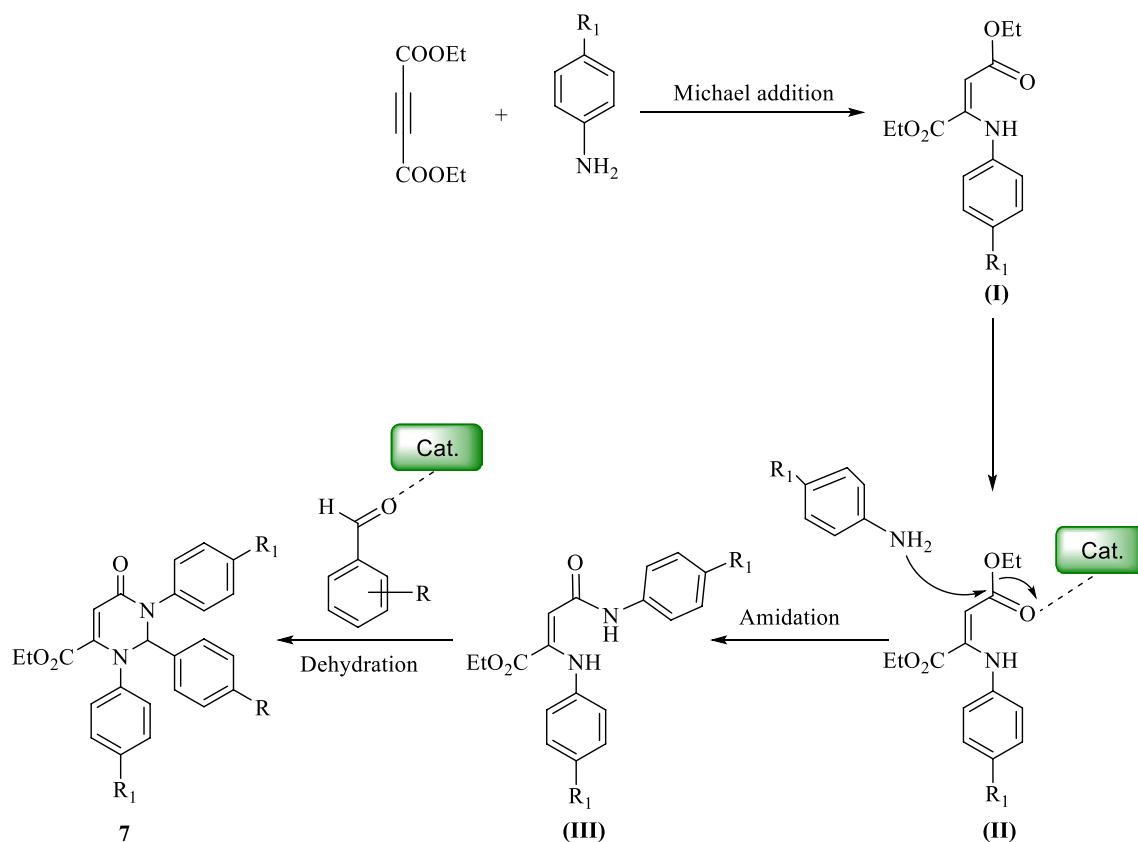


Figure 12. Proposed mechanism 2-amino-4H-chromenes synthesis in the presence of the catalyst.

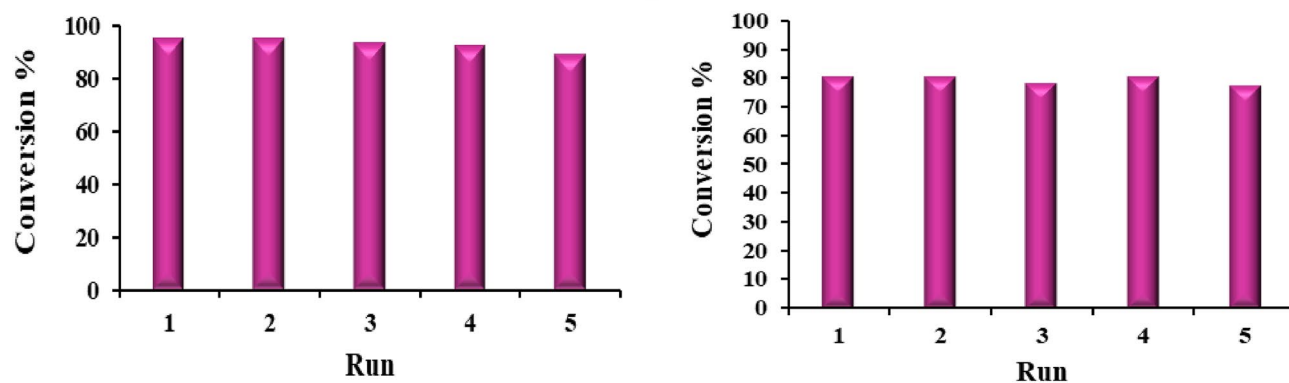


Figure 13. Recyclability of the catalyst in 2-amino-4H-chromene (left) and 1,2,3,6- tetrahydropyrimidine (right) synthesis model reaction.

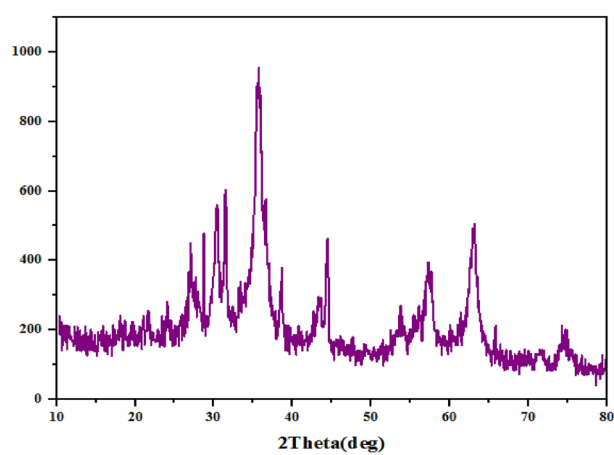


Figure 14. XRD of recycled catalyst after 5 runs.

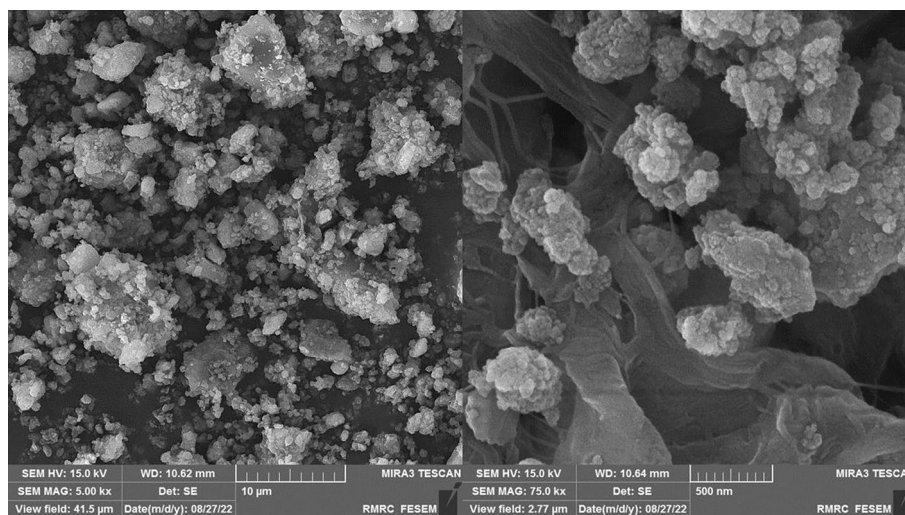


Figure 15. SEM images of recycled catalyst.

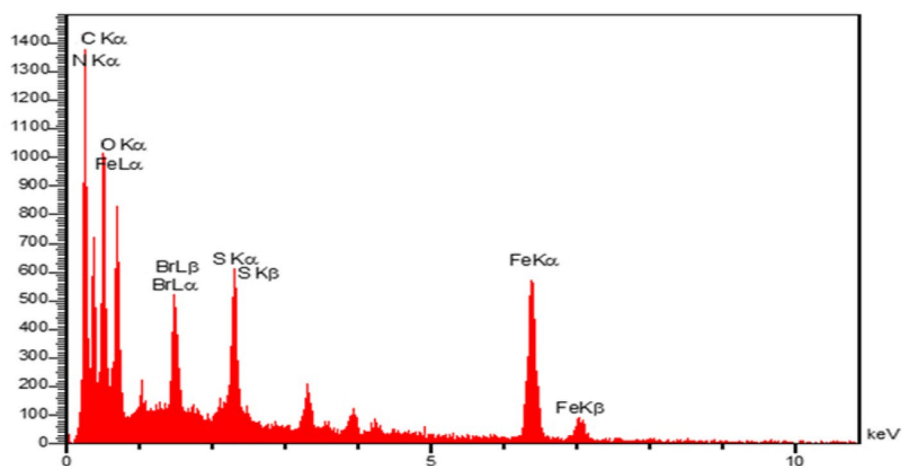


Figure 16. EDS spectra of recycled catalyst.

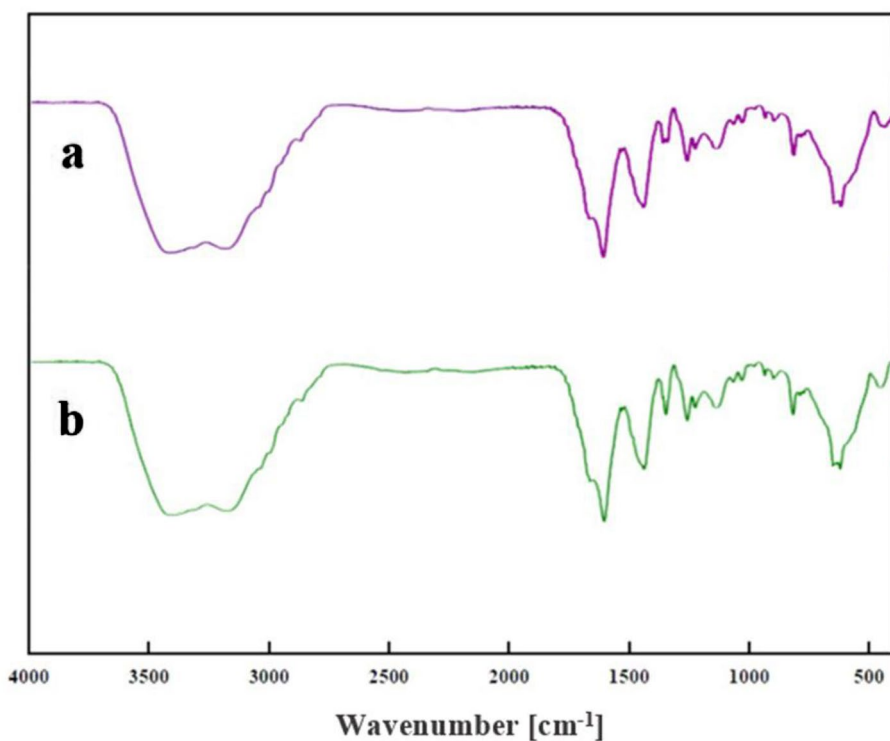


Figure 17. The FT-IR spectra of (a) catalyst, (b) recycled catalyst.

Availability of data and materials

All data generated or analysed during this study are included in this published article [and its supplementary information files].

Received: 7 August 2023; Accepted: 18 November 2023

Published online: 23 November 2023

References

1. Ganjali, F., Kashtiaray, A., Zarei-Shokat, S., Taheri-Ledari, R. & Maleki, A. Functionalized hybrid magnetic catalytic systems on micro- and nanoscale utilized in organic synthesis and degradation of dyes. *Nanoscale Adv.* **4**, 1263–1307 (2020).
2. Rashidzadeh, A., Ghafuri, H., Esmaili Zand, H. R. & Goodarzi, N. Graphitic carbon nitride nanosheets covalently functionalized with biocompatible vitamin B1: Synthesis, characterization, and its superior performance for synthesis of quinoxalines. *ACS Omega* **4**, 12544–12554 (2019).

3. Liu, J., Lei, M. & Hu, L. Thiamine hydrochloride (VB₁): An efficient promoter for the one-pot synthesis of benzo[4,5]imidazo[1,2-*a*]pyrimidine and [1,2,4]triazolo[1,5-*a*]pyrimidine derivatives in water medium. *Green Chem.* **14**, 840–846 (2012).
4. Chen, Y. & Zhang, X. P. Vitamin B₁₂ derivatives as natural asymmetric catalysts: Enantioselective cyclopropanation of alkenes. *J. Org. Chem.* **69**, 2431–2435 (2004).
5. Lei, M., Ma, L. & Hu, L. Highly chemoselective condensation of β-naphthol, aldehyde, and urea catalyzed by thiamine hydrochloride. *Synth. Commun.* **41**, 3424–3432 (2011).
6. Yi, Z. *et al.* Green and efficient cycloaddition of CO₂ toward epoxides over thiamine derivatives/GO aerogels under mild and solvent-free conditions. *Sci. China Chem.* **60**, 990–996 (2017).
7. Lam, E. & Luong, H. T. Carbon materials as catalyst supports and catalysts in the transformation of biomass to fuels and chemicals. *ACS Catal.* **4**, 3393–3410 (2014).
8. Dubertret, B., Heine, T. & Terrones, M. The rise of two-dimensional materials. *Acc. Chem. Res.* **48**, 1–2 (2015).
9. Ong, W. J., Tan, L. L., Ng, Y. H., Yong, S. T. & Chai, S. P. Graphitic carbon nitride (g-C₃N₄)-based photocatalysts for artificial photosynthesis and environmental remediation: Are we a step closer to achieving sustainability?. *Chem. Rev.* **116**, 7159–7329 (2016).
10. Zhang, Y. *et al.* Protic salts of high nitrogen content as versatile precursors for graphitic carbon nitride: Anion effect on the structure, properties, and photocatalytic activity. *ChemPlusChem.* **80**, 1139–1147 (2015).
11. Zhuang, X., Mai, Y., Wu, D., Zhang, F. & Feng, X. Two-dimensional soft nanomaterials: A fascinating world of materials. *Adv. Mater.* **27**, 403–427 (2015).
12. Zheng, Y., Lin, L., Ye, X., Guo, F. & Wang, X. Helical graphitic carbon nitrides with photocatalytic and optical activities. *Angew. Chem. Int. Ed.* **126**, 12120–12124 (2014).
13. Li, C. Z., Wang, Z. B., Sui, X. L., Zhang, L. M. & Gu, D. M. Ultrathin graphitic carbon nitride nanosheets and graphene composite material as high-performance PtRu catalyst support for methanol electro-oxidation. *Carbon* **93**, 105–115 (2015).
14. Gong, Y. *et al.* A novel catalyst Pd@ompg-C₃N₄ for highly chemoselective hydrogenation of quinoline under mild conditions. *J. Catal.* **297**, 272–280 (2013).
15. Huang, Y. *et al.* Preparation of 2D hydroxyl-rich carbon nitride nanosheets for photocatalytic reduction of CO₂. *RSC Adv.* **5**, 33254–33261 (2015).
16. Vattikuti, S. V. P., Reddy, P. A. K., Shim, J. & Byon, C. Visible-light-driven photocatalytic activity of SnO₂-ZnO quantum dots anchored on g-C₃N₄ nanosheets for photocatalytic pollutant degradation and H₂ production. *ACS Omega* **3**, 7587–7602 (2018).
17. Zhong, Y. *et al.* CdSe quantum dots/g-C₃N₄ heterostructure for efficient H₂ production under visible light irradiation. *ACS Omega* **3**, 17762–17769 (2018).
18. Bahuguna, A., Choudhary, P., Chhabra, T. & Krishnan, V. Ammonia-doped polyaniline-graphitic carbon nitride nanocomposite as a heterogeneous green catalyst for synthesis of indole-substituted 4H-chromenes. *ACS Omega* **3**, 12163–12178 (2018).
19. Gong, Y., Li, M., Li, H. & Wang, Y. Graphitic carbon nitride polymers: Promising catalysts or catalyst supports for heterogeneous oxidation and hydrogenation. *Green Chem.* **17**, 715–736 (2015).
20. Barrio, J. & Shalom, M. Rational design of carbon nitride materials by supramolecular preorganization of monomers. *ChemCatChem.* **10**, 5573–5586 (2018).
21. Shahabi, S. S., Azizi, N. & Vatanpour, V. Synthesis and characterization of novel g-C₃N₄ modified thin film nanocomposite reverse osmosis membranes to enhance desalination performance and fouling resistance. *Sep. Purif. Technol.* **215**, 430–440 (2019).
22. Fu, Y., Zhu, J., Hu, C., Wu, X. & Wang, X. Covalently coupled hybrid of graphitic carbon nitride with reduced graphene oxide as a superior performance lithium-ion battery anode. *Nanoscale* **6**, 12555–12564 (2014).
23. Wang, Y. *et al.* Boronic acid functionalized g-C₃N₄ nanosheets for ultrasensitive and selective sensing of glycoprotein in physiological environment. *Nanoscale* **10**, 4913–4920 (2018).
24. Sun, J. *et al.* Covalent functionalization of carbon nitride frameworks through cross-coupling reactions. *Chem. Eur. J.* **24**, 14921–14927 (2018).
25. Chauhan, D. K., Jain, S., Battula, V. R. & Kailasam, K. Organic motifs functionalization via covalent linkage in carbon nitride: An exemplification in photocatalysis. *Carbon* **152**, 40–58 (2019).
26. Kumru, B. *et al.* Robust carbon nitride based thermoset coatings for surface modification and photochemistry. *ACS Appl. Mater. Interfaces.* **11**, 9462–9469 (2019).
27. Di, J. Q. *et al.* Copper anchored on phosphorus g-C₃N₄ as a highly efficient photocatalyst for the synthesis of N-arylpyridin-2-amines. *Green Chem.* **23**, 1041–1049 (2021).
28. Coppola, A. *et al.* Multicomponent reactions and photo/electrochemistry join forces: Atom economy meets energy efficiency. *Chem. Soc. Rev.* **51**, 2313–2382 (2022).
29. Daraie, M., Heravi, M. M., Mohammadi, P. & Daraie, A. Silver incorporated into g-C₃N₄/Alginate as an efficient and heterogeneous catalyst for promoting click and A³ and KA² coupling reaction. *Sci. Rep.* **11**, 1–13 (2021).
30. Hassankhani, A., Gholipour, B. & Rostamnia, S. An efficient regioselective three-component synthesis of tetrazoloquinazolines using g-C₃N₄ covalently bonded sulfamic acid. *Polyhedron* **175**, 30662–30681 (2020).
31. Kamali, F. & Shirini, F. An efficient one-pot multi-component synthesis of spirooxindoles using Fe₃O₄/g-C₃N₄ nanocomposite as a green and reusable catalyst in aqueous media. *J. Mol. Struct.* **1227**, 129654–129686 (2021).
32. Choudhary, P. *et al.* Sulfonic acid functionalized graphitic carbon nitride as solid acid–base bifunctional catalyst for Knoevenagel condensation and multicomponent tandem reactions. *Mater. Chem. Front.* **5**, 6265–6278 (2021).
33. Neamani, S. & Moradi, L. Loading of g-C₃N₄ on core-shell magnetic mesoporous silica nanospheres as a solid base catalyst for the green synthesis of some chromene derivatives under different conditions. *ChemistryOpen.* **11**, 2022000041 (2022).
34. Gao, G., Di, J. Q., Zhang, H. Y., Mo, L. P. & Zhang, Z. H. A magnetic metal organic framework material as a highly efficient and recyclable catalyst for synthesis of cyclohexenone derivative. *J. Catal.* **387**, 39–46 (2020).
35. Wanga, Y. M., Li, W. J., Wang, M. M., Zhang, M. & Zhang, Z. H. Magnetic MoS₂ as an efficient heterogeneous photocatalyst for α-methoxymethylation and aminomethylation of aromatic ketones. *Catal. Sci. Technol.* **13**, 665–674 (2023).
36. Zhang, M., Liu, Y. H., Shang, Z. R., Hu, H. C. & Zhang, Z. H. Supported molybdenum on graphene oxide/Fe₃O₄: An efficient, magnetically separable catalyst for one-pot construction of spiro-oxindole dihydropyridines in deep eutectic solvent under microwave irradiation. *Catal. Commun.* **8**, 39–44 (2017).
37. Xu, L., Zhang, S. Z., Li, W. & Zhang, Z. H. Visible-light-mediated oxidative amidation of aldehydes by using magnetic CdS quantum dots as a photocatalyst. *Chem. Eur. J.* **27**, 5483–5491 (2021).
38. Deng, Q., Shen, Y., Zhu, H. & Tu, T. A magnetic nanoparticle-supported n-heterocyclic carbene-palladacycle: An efficient and recyclable solid molecular catalyst for suzuki-miyaura cross-coupling of 9-chloroacridine. *Chem. Commun.* **53**, 13063–13066 (2017).
39. Wang, Q. *et al.* Hierarchical-structured Pd nanoclusters catalysts x-PdNCs/CoAl(O)/rGO-T by the captopril-Capped Pd cluster precursor method for the highly efficient 4-Nitrophenol reduction. *ACS Appl. Mater. Interfaces.* **14**, 27775–27790 (2022).
40. Patil, A. *et al.* New substituted 4H-chromenes as anticancer agents. *Bioorgan. Med. Chem. Lett.* **22**, 4458–4461 (2012).
41. Kumar, D., Reddy, V. B., Sharad, S., Dube, U. & Kapur, S. A facile one-pot green synthesis and antibacterial activity of 2-amino-4H-pyrans and 2-amino-5-oxo-5, 6, 7, 8-tetrahydro-4H-chromenes. *Eur. J. Med. Chem.* **44**, 3805–3809 (2009).
42. Gu, J. *et al.* Synthesis, crystal structure, spectroscopic characterization and anti-fungal activity of ethyl 2-Oxo-2H-chromene-3-carboxylate derivatives. *J. Mol. Struct.* **1257**, 132576 (2022).

43. Eivazzadeh-Keihan, R., Bahrami, S., Ghafori Gorab, M., Sadat, Z. & Maleki, A. Functionalization of magnetic nanoparticles by creatine as a novel and efficient catalyst for the green synthesis of 2-amino-4H-chromene derivatives. *Sci. Rep.* **12**, 10664 (2022).
44. Bahrami, S., Hassanzadeh-Afruzi, F. & Maleki, A. Synthesis and characterization of a novel and green rod-like magnetic ZnS/CuFe₂O₄/agar organometallic hybrid catalyst for the synthesis of biologically-active 2-amino-tetrahydro-4H-chromene-3-carbonitrile derivatives. *Appl. Organomet. Chem.* **34**, 5949 (2020).
45. Wanzheng, M. A., Ebadi, A. G., Shahbazi Sabil, M., Javahershenas, R. & Jimenez, G. One-pot synthesis of 2-amino-4H-chromene derivatives by MNPs@Cu as an effective and reusable magnetic nanocatalyst. *RSC Adv.* **9**, 12801–12812 (2019).
46. Bayzidi, M. & Zeynizadeh, B. The immobilized zirconocene chloride on magnetite-reduced graphene oxide: A highly efficient and reusable heterogeneous nanocatalyst for one-pot three-component synthesis of tetrahydrobenzo[b]pyrans and dihydropyrano[3,2-c]chromenes. *ChemistrySelect.* **7**, 202202708 (2022).
47. Rezvanian, A., Khodadadi, B. & Tafreshi, S. Use of dialkyl acetylenedicarboxylates in the multicomponent synthesis of heterocyclic structures. *ChemistrySelect.* **7**, 202202360 (2022).
48. Habibi-Khorassani, S. M., Shahraki, M., Dehdab, M. & Poorshamsoddin, M. A. Kinetic and mechanistic elucidation of the formation reaction of 3,4,5-substituted furan-2(5H)-ones in formic acid as the solvent. *J. Solut. Chem.* **44**, 2154–2166 (2015).
49. Shahraki, M., Habibi-Khorassani, S. M. & Dehdab, M. Effect of different substituents on the one-pot formation of 3,4,5-substituted furan-2(5H)-ones: A kinetics and mechanism study. *RSC Adv.* **5**, 52508–52515 (2015).
50. Zhang, M. & Jiang, H. F. A new multicomponent reaction catalyzed by a Lewis acid catalyst: Convenient synthesis of polyfunctional tetrahydropyrimidines. *Eur. J. Org. Chem.* **2008**, 3519–3523 (2008).
51. Pattarini, R., Smeyne, R. J. & Morgan, J. I. Temporal mRNA profiles of inflammatory mediators in the murine 1-methyl-4-phenyl-1,2,3,6-tetrahydropyrimidine model of Parkinson's disease. *Neuroscience* **145**, 654–668 (2007).
52. Kumar, A. S. K. *et al.* Magnetically separable nanospherical g-C₃N₄@Fe₃O₄ as a recyclable material for chromium adsorption and visible-light-driven catalytic reduction of aromatic nitro compounds. *ACS Sustain. Chem. Eng.* **7**, 6662–6671 (2019).
53. Abbaspour-Gilandeh, E., Aghaei-Hashjin, M., Yahyazadeh, A. & Salemi, H. (CTA)₃[SiW₁₂]-Li⁺-MMT: a novel, efficient and simple nanocatalyst for facile and one-pot access to diverse and densely functionalized 2-amino-4H-chromene derivatives via an eco-friendly multicomponent reaction in water. *RSC Adv.* **6**, 55444–55462 (2016).
54. Singh, P., Yadav, P., Mishra, A. & Awasthi, K. S. Green and mechanochemical one-pot multicomponent synthesis of bioactive 2-amino-4H-benzo[b]pyrans via highly efficient amine-functionalized SiO₂@Fe₃O₄ nanoparticles. *ACS Omega* **5**, 4223–4232 (2020).
55. Zolfigol, M. A., BahramiNejad, N., Afsharnadery, F. & Bagheri, S. 1-Methylimidazolium tricyanomethanide [HMIM]C(CN)₃ as a nano structure and reusable molten salt catalyst for the synthesis of tetrahydrobenzo[b]pyrans via tandem Knoevenagel-Michael cyclocondensation and 3,4-dihydropyrano[c]chromene derivatives. *J. Mol. Liq.* **221**, 851–859 (2016).
56. Azizi-Amiri, M. R., Firouzzadeh-Pasha, G., Tajbakhsh, M. & Asghari, S. Copper-amine complex immobilized on nano NaY zeolite as a recyclable nanocatalyst for the environmentally friendly synthesis of 2-amino-4H-chromenes. *Appl. Organomet. Chem.* **36**, 8668 (2022).
57. Noori-Sadeh, F., Maghsoodlou, M. T., Hazeri, N. & Kangani, M. A facile and efficient synthesis of tetrahydrobenzo[b]pyrans using lactose as a green catalyst. *Res. Chem. Intermed.* **41**, 5907–5914 (2015).
58. Tamimi, M. *et al.* Ag₃[PMo₁₂O₄₀]: An efficient and green catalyst for the synthesis of highly functionalized pyran-annulated heterocycles via multicomponent reaction. *Appl. Organomet. Chem.* **33**, 5043 (2019).
59. Ghamari Kargar, P., Bagherzade, G. & Eshghi, H. Novel biocompatible core/shell Fe₃O₄@NFC@Co(II) as a new catalyst in a multicomponent reaction: An efficient and sustainable methodology and novel reusable material for one-pot synthesis of 4H-pyran and pyranopyrazole in aqueous media. *RSC Adv.* **10**, 37086–37097 (2020).
60. Kiyani, H. & Ghorbani, F. Efficient tandem synthesis of a variety of pyran-annulated heterocycles, 3,4-disubstituted isoxazol-5(4H)-ones, and α,β-unsaturated nitriles catalyzed by potassium hydrogen phthalate in water. *Res. Chem. Intermed.* **41**, 7847–7882 (2015).
61. Tu, S. *et al.* A facile and efficient synthesis of new polysubstituted indeno[1,2-b]pyridines via one-pot, three-component microwave-assisted reaction. *Synlett* **3**, 480–484 (2007).
62. Hosseinzadeh-Baghan, S. *et al.* An inorganic-organic hybrid material based on a Keggin-type polyoxometalate@Dysprosium as an effective and green catalyst in the synthesis of 2-amino-4H-chromenes via multicomponent reactions. *Appl. Organomet. Chem.* **34**, 5793 (2020).
63. Kamali, F. & Shirini, F. Melamine: An efficient promoter for some of the multi-component reactions. *Polycycl. Aromat. Compd.* **41**, 73–94 (2019).
64. Joshi, M. V. *et al.* Novel one-pot synthesis of 4H-chromene derivatives using amino functionalized silica gel catalyst. *Chin. Chem. Lett.* **25**, 455–458 (2014).
65. Kamalzare, M., Bayat, M. & Maleki, A. Green and efficient three-component synthesis of 4H-pyran catalysed by CuFe₂O₄@starch as a magnetically recyclable bionanocatalyst. *R. Soc. Open Sci.* **7**, 200385 (2020).
66. Kisomi, P. R., Shirini, F. & Golshekan, M. Introduction of organic/inorganic Fe₃O₄@MCM-41@Zr-piperazine magnetite nanocatalyst for the promotion of the synthesis of tetrahydro-4H-chromene and pyrano[2,3-d]pyrimidinone derivatives. *Appl. Organomet. Chem.* **32**, 4371 (2018).
67. Ramesh, R., Vadivel, P., Maheswari, S. & Lalitha, A. Click and facile access of substituted tetrahydro-4H-chromenes using 2-aminopyridine as a catalyst. *Res. Chem. Intermed.* **42**, 7625–7636 (2016).
68. Moghaddam, M. F., Eslami, M. & Hoda, G. Cysteic acid grafted to magnetic graphene oxide as a promising recoverable solid acid catalyst for the synthesis of diverse 4H-chromene. *Sci. Rep.* **10**, 20968 (2020).

Acknowledgements

We are grateful for the scientific and financial support of Research Council University of Mazandaran.

Author contributions

Writing: F.R.; B.M. Conceptualization: F.R.; B.M. H. A. Data curation: F.R.; B.M. H. A. Formal analysis: F.R.; B.M. H. A. Project administration: F.R.; B.M. H. A. Methodology: F.R. Validation: F.R.; B.M. H. A. Review and editing: B.M. H. A.

Competing interests

The authors declare that they have no known competing financial interests or personal relationships that could have appeared to influence the work reported in this paper.

Additional information

Supplementary Information The online version contains supplementary material available at <https://doi.org/10.1038/s41598-023-47794-2>.

Correspondence and requests for materials should be addressed to H.A. or B.M.

Reprints and permissions information is available at www.nature.com/reprints.

Publisher's note Springer Nature remains neutral with regard to jurisdictional claims in published maps and institutional affiliations.



Open Access This article is licensed under a Creative Commons Attribution 4.0 International License, which permits use, sharing, adaptation, distribution and reproduction in any medium or format, as long as you give appropriate credit to the original author(s) and the source, provide a link to the Creative Commons licence, and indicate if changes were made. The images or other third party material in this article are included in the article's Creative Commons licence, unless indicated otherwise in a credit line to the material. If material is not included in the article's Creative Commons licence and your intended use is not permitted by statutory regulation or exceeds the permitted use, you will need to obtain permission directly from the copyright holder. To view a copy of this licence, visit <http://creativecommons.org/licenses/by/4.0/>.

© The Author(s) 2023